Journal of Applied Polymer Science

Enhanced Dispersion of Lignin in Epoxy Composites Through Hydration and Mannich Functionalization

Gamini P. Mendis,[1] Inez Hua,[2,3] Jeffrey P. Youngblood,[1] John A. Howarter[1,3]
[1]School of Materials Engineering, Purdue University, West Lafayette, Indiana 47907
[2]School of Civil Engineering, Purdue University, West Lafayette, Indiana 47907
[3]Division of Environmental and Ecological Engineering, Purdue University, West Lafayette, Indiana 47907
Correspondence to: J. A. Howarter (E-mail: howarter@purdue.edu)

ABSTRACT: Lignin was used as a biobased fill material to create epoxy composites. Lignin was incorporated into diglycidyl ether of bisphenol A–based epoxy using hydration and Mannich functionalization. The effects of chemical functionalization on the interfacial chemistry of lignin are examined, and the corresponding changes in materials properties are examined. Several types of lignin–epoxy composites were formed through dissolution of lignin in aliphatic amine. Lignin–amine solutions were modified through hydration and the Mannich reaction and were used to cure the epoxy. The resulting composites exhibited two-phase microstructures containing lignin-rich agglomerates. Thermomechanical properties were examined using dynamic mechanical analysis, differential scanning calorimetry, and fracture testing. Morphological and chemical changes were examined using scanning electron microscopy and Fourier transform infrared spectroscopy. The hydrated lignin samples showed similar glass transitions and mechanical properties to the neat epoxy samples. Interactions between water and the Mannich functionalized lignin decreased the glass transition temperature and mechanical properties of the highly hydrated Mannich reacted lignin samples because of a plasticization effect. Fracture testing was conducted on the samples and showed that the yield strength and elastic modulus were similar to the neat epoxy, but the fracture toughness decreased in the lignin-containing specimen. © 2014 Wiley Periodicals, Inc. J. Appl. Polym. Sci. **2015**, *132*, 41263.

KEYWORDS: biopolymers and renewable polymers; cellulose and other wood products; differential scanning calorimetry (DSC); glass transition; structure-property relations

Received 7 May 2014; accepted 8 July 2014
DOI: 10.1002/app.41263

INTRODUCTION

Lignin is one of the three main components of wood and is an underutilized byproduct of the papermaking industry.[1] Approximately 50 million tons of lignin are produced annually. However, only 2% of this is used for commercial applications, with the remaining lignin being burned for low-grade fuel.[1] Lignin is commercially produced through two different sulfur-based processes, the Sulfite process and the Kraft process, which create lignosulfonate lignin and Kraft lignin, respectively. Although 95% of the lignin is produced through the Kraft process, it comprises only about 10% of the commercial demand for lignin,[1] stressing the need for more value-added Kraft lignin applications. The abundance and low cost of industrially produced lignin makes it a promising renewable feedstock material for chemical processes.[2] However, the use of lignin in engineering applications is limited because of process impurities, such as sulfur contamination, and physiochemical inhomogeneity arising from feedstock differences. A key material processing limitation with using lignin in engineering applications is the difficulty in incorporating lignin into common polymers.[2]

Lignin is often described as a phenylpropane-based, 3D polymer, composed of three major units, guaiacyl, syringyl, and *p*-coumaryl alcohol,[3] in different proportions according to the extraction method and plant source.[4] These structural units are composed of crosslinked mono- and di-substituted phenolic hydroxyl and methoxy groups,[5] which strongly affect the properties of the lignin molecule. The large number of interfacial chemistries and the naturally crosslinked structure of lignin are significant barriers to incorporating lignin into high-value engineering applications.

To surmount these barriers, lignin has been used as reinforcement in polymeric systems, through various chemical functionalizations. Significant research has been done to incorporate lignin into poly(lactic acid),[6–8] poly(vinyl acetate),[9] phenol–formaldehyde,[8] and urea–formaldehyde resins,[10] to enhance mechanical and flame retarding properties, but aggregation is still a significant problem in certain polymer systems. Pouteau et al.[11,12] examined lignin aggregation in 12 different polymers with varying solubility parameters and found that decreased

Table I. Compositions and Abbreviations of Epoxy Samples

Specimen name	Epoxy (wt %)	Lignin (wt %)	TETA (wt %)	Water (wt %)	Form. (wt %)
Neat (Neat)	87.8		12.2		
Immediate (IMM)	86.9	1.2	12.1		
Hydration low (HL)	85.1	0.8	11.9	1.7	
Hydration high (HH)	79.6	1.1	11.1	7.9	
Mannich low (ML)	85.1	0.8	11.9	1.5	0.2
Mannich high (MH)	79.6	1.1	11.1	7.1	0.7
Mannich rehydrated low (MRL)	85.1	0.8	11.9	1.5/7[a]	0.2
Mannich rehydrated high (MRH)	79.6	1.1	11.1	7.1/7.9[a]	0.7

[a] Water added postextraction.

molecular weight of the lignin increased dispersion. Lignin has been incorporated into other polymer systems through grafting of styrene and methyl–methacrylate branches via atom transfer radical polymerization,[13] although agglomeration is still seen.

Previous work has investigated processing and material properties of various epoxy–lignin formulations. In a series of studies, the cure kinetics and mechanical properties of an epoxidized lignin–poly(propylene oxide) blend were characterized.[14–16] Epoxy–lignin polyblends were also examined through adhesive testing,[17] thermal properties,[18] and cure kinetics,[19] showing that lignin can be incorporated into epoxy.

This study was designed to examine the degree of incorporation of lignin into epoxy using two simple processing methodologies, with the goal of creating a viable end-of-life alternative for lignin while maintaining the properties of the epoxy. To overcome problems with lignin solubility in epoxy, two simple methods are examined: the hydration of a lignin–amine solution and the functionalization of lignin using the Mannich reaction (Figure 1).[20–22] Modified lignin is mixed into epoxy and thermally cured. The structure–property relationships are examined through comparisons between morphological and chemical analysis and the resulting mechanical properties. The physical and chemical properties were probed using dynamic mechanical analysis (DMA), differential scanning calorimetry (DSC), fracture testing, Fourier transform infrared spectroscopy (FTIR), nuclear magnetic resonance (NMR) spectroscopy, and scanning electron microscopy (SEM). Ideal samples should show macroscopically single phase morphologies with fully dispersed lignin, increased glass transition temperature and similar mechanical properties. Chemical modification and degree of hydration were identified as key parameters which controlled dispersion and thermomechanical properties. Functionalization through the Mannich reaction increases the compatibility of lignin with epoxy through increased surface chemistry changes caused by lignin–amine interactions. Hydration of the lignin in amine causes deprotination of the hydroxyl which increases dispersion of the lignin in epoxy.

EXPERIMENTAL

Materials

Diglycidyl ether of bisphenol A (DGEBA, epoxide equivalent weight 172–176, viscosity 4000–6000 cps), triethylene tetramine (TETA), and kraft lignin [characterized using 1H-NMR, see below, methylene (5.5%, 0.8–1.3 ppm), aliphatic (39%, 3.5–4.0 ppm), aliphatic hydroxyl (15.5%, 4.1–5.7 ppm), aromatic (34.2%, 6.0–7.7 ppm), aromatic hydroxyl (5.8%, 8.3–9.3)] were obtained from Sigma Aldrich (St. Louis, MO); methyl ethyl ketone (99.8%) and formaldehyde (38% in solution) were obtained from Mallinckrodt (Paris, KY) and deionized water (18.3 M-ohm/cm) was purified in-house using a Barnstead Nanopure system (Dubuque, IA). Silicone molds were prepared with Mold Max 60 (Smooth-On, Easton, PA).

The neat epoxy samples were prepared by mixing 13 wt % TETA hardener with DGEBA resin. The uncured epoxy mixture was then stirred at 550 rpm for 15 min. The liquid epoxy was then poured into silicone molds and was degassed in vacuum for 10 min. Samples were cured at room temperature for 24 h, followed by a ramp up to 100°C at a heating rate of 0.83°C/min. Samples were held at 100°C for 4 h and then removed to ambient temperature to cool. All sample formulations described below followed the same processing protocol once the hardener and resin were mixed. Table I shows the compositions of each sample. The process for varying the epoxy composition is described below.

A lignin-hardener solution was prepared by adding 10 wt % lignin to TETA. The lignin and TETA homogenized quickly, and as a result, initial samples were only stirred for 5 min (sample designated as 'Immediate or IMM' in this document). All other samples were stirred for 1 h in sealed glass vials followed by addition of a modifying agent to increase compatibility. For two sample formulations (hydration high, HH and hydration low, HL), deionized water was added at a rate of 0.1 g/min to the lignin–TETA solution. For two sample formulations (Mannich low, ML and Mannich high, MH), formaldehyde solution was added at a rate of 0.1 g/min to lignin–TETA solutions to prevent localized crosslinking and the large exotherm during the Mannich reaction. The formaldehyde was completely consumed in the reaction. To test the difference between hydration and Mannich functionalization, Mannich-rehydrated solutions (Mannich-rehydrated low, MRL and Mannich-rehydrated high, MRH) were subjected to a controlled water extraction, using methyl ethyl ketone to segregate water and a rotary evaporator to fully remove water. Known quantities of water were then added to the Mannich-processed lignin–TETA solutions.

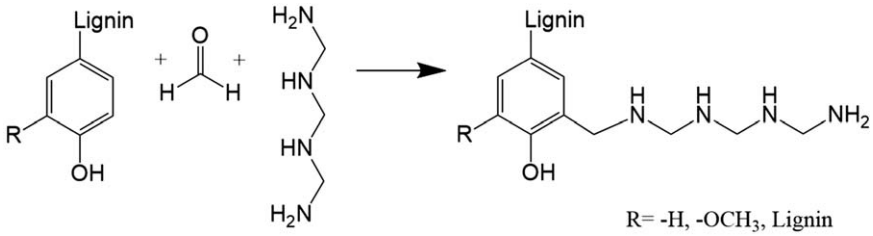

Figure 1. Synthesis scheme of a Mannich-functionalized lignin molecule.[20] Unbonded nitrogen atoms can react with epoxy molecules to form a cured epoxy resin.

Material Characterization

The as-received lignin was dissolved in dimethyl sulfoxide and an ^{1}H-NMR spectra was taken using eight scans with a Bruker ARX400 NMR.

The epoxy samples were characterized using a Spectrum 100 FTIR (Perkins Elmer, Waltham, MA), a Q2000 Differential Scanning Calorimeter (TA Instruments, Newcastle, DE), Q800 Dynamic Mechanical Analyzer (TA instruments), and S-4800 Field Emission Scanning Electron Microscope (Hitachi High-Technologies Corporation, Schaumburg, IL). FTIR was used to determine chemical composition of the epoxy samples. A powdered sample was obtained by scraping a razor blade over the surface of the sample. Sample powder (2 ± 0.2 mg) was separately mixed into 300 mg potassium bromide (KBr), then dried overnight at 120°C and pressed into a 20-mg pellet. The samples were mounted in transmission mode using 16 scans. Glass transition and curing information was obtained using DSC. Samples were massed (8.8 ± 0.4 mg) and placed in aluminum sample pans (TA instruments). DSC thermograms were prepared using a heat–cool–heat cycle beginning at 0°C, ramping to 200°C at 10°C/min, cooling to 0°C at 5°C/min, and heating again to 200°C at 10°C/min. DMA was used to characterize the thermomechanical properties and glass transition. Samples were prepared by grinding the surface to approximately 35 mm × 2 mm × 12 mm. Samples were mounted in a Dual Cantilever apparatus and were allowed to equilibrate at 40°C for 5 min before ramping to 180°C at 10°C/min and 1 Hz. Sample cross-sections were mounted in Bakelite, polished using silicon carbide paper and colloidal alumina and then cleaned with water and ethanol. Fracture surfaces and cross-sections were sputtered with gold palladium for 90 s using a sputter coater. SEM imaging was performed using an S-4800 Field Emission at 5 kV and a 10-mm working distance.

Fracture Testing

Samples were prepared according to ASTM D5045, using the three-point bend sample geometry. Specimens were sectioned using a Universal Laser Systems PLS 3.60 laser cutter (Amtek Company, Arnold, MD) at 30% intensity and 40% speed to create bars of approximately 10 mm × 5 mm × 44 mm. Notches were cut using a Diamond Laser 5000 band saw (Diamond Tech, Tampa, FL), and a razor blade was used to create a sharp crack. Samples were tested according to ASTM D5045 using a Sintech 30/D (MTS, Eden Prairie, MN) tensile tester at a rate of 10 mm/min at 23°C with a 2000-N load cell and a three-point bend fixture.

RESULTS AND DISCUSSION

Initially, unmodified kraft lignin showed no dispersion when added to water. After dissolution in amine, the lignin–amine solution readily dissolved into water, indicating a change in hydrophilicity. The Mannich-functionalized lignin showed similar dissolution in water. Fast addition of Mannich-functionalized lignin and lignin–amine solution to water created noticeable exothermic reactions. Through preliminary testing, hydration of both the lignin–amine solution and the Mannich-functionalized lignin was empirically found to increase compatibility with epoxy. Without the hydration step, large lignin agglomerates could be seen in the uncured epoxy mixture similar in morphology to the IMM samples [Figure 2(A)].

Phase separation of the lignin was not seen upon mixing of the epoxy and TETA solutions; however, small, lignin-rich pools have been observed during the degassing step. Phase separation

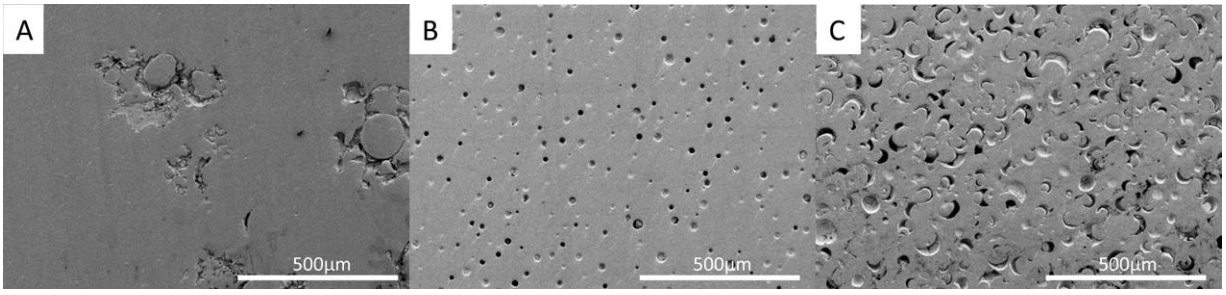

Figure 2. Three representative SEM micrographs of sample cross-sections. Microstructures shown are representative of the Neat and IMM samples (Inset A), the HL, HH, ML, and MH samples (Inset B), and the MRL, MRH samples (Inset C). Micrographs shown were taken of the underlined samples.

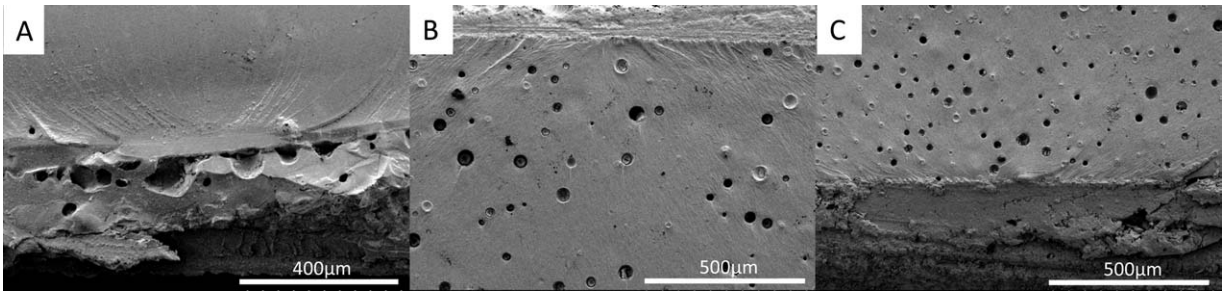

Figure 3. Three representative SEM micrographs of fracture surfaces. Microstructures shown are representative of the Neat and IMM samples (Inset A), the HL, HH samples (Inset B) and the ML, MRL samples (Inset C). Micrographs shown were taken of the underlined samples.

is not strongly observed in the room temperature curing samples, which appear homogeneously dark brown. However, upon postcuring, second-phase particles are visible in the lignin-containing samples.

At increased temperature, three mechanisms may cause formation and subsequent debonding of the second phase (1) lignin islands exist at room temperature and initially are in equilibrium with the epoxy matrix, but thermal energy causes liquid solvent loss either by evaporation or migration through the epoxy, so that the previously swelled particle shrinks and cracks, (2) the lignin islands form an equiaxed solid phase with the epoxy at high temperatures, which, upon cooling, debonds as a result of thermal stresses induced by differences in coefficient of thermal expansion or (3) lignin islands form at room temperature and creates a sphere in equilibrium with the epoxy matrix, which, upon heating, compressively stresses the epoxy surrounding the void. The differences in the coefficient of thermal expansion between the matrix and the lignin islands likely contribute to the cracking of the island and its subsequent debonding.

The morphologies of the lignin-containing epoxy samples exhibited marked differences because of the presence of lignin-rich second phases (Figure 2). The Neat sample exhibited a largely featureless, homogeneous microstructure, similar to the lower left region shown in Figure 2(A). The IMM sample [Figure 2(A)] was largely homogeneous, but also contained localized lignin agglomerates, as shown in the lower right of the image. The HL, HH, ML, and MH all exhibited the presence of a second phase consisting of equiaxed, spherical pores encapsulated by lignin [Figure 2(B)]. The areal density of the pores and the size of the pores increased with the amount of water in the sample. The MRL and MRH samples [Figure 2(C)] displayed a randomly oriented, crescent-like second phase, which became denser with higher water content.

The fracture surfaces of the samples (Figure 3) show similar microstructural features to the cross-sections (Figure 2). All specimen show similar degrees of brittle fracture as shown in Figure 3; however, the morphology of the lignin containing samples differ from the neat samples. The Neat and IMM samples show a largely homogeneous microstructure; however, the lignin agglomerates strongly in the IMM sample, creating large clusters. In the HL, HH, ML, and MRL samples, the spherical lignin-rich second phase can be seen, similar to the SEM cross-sections. The size and density of the second phase vary monotonically with the amount of water in the specimen.

Crater-like features are also apparent in the fracture samples, which are likely to be the lignin-rich second phases that formed a hollow sphere inside the pores and collapsed upon fracture. These crater-like features are on a similar size scale to the pores in the cross-sectional micrographs. The crater-like features do not appear in the SEM cross-sections, likely because water dissolved the features during the polishing step. When polishing the cross-section specimen, water is used to pull away excess material; when the samples were exposed to water, a viscous brown liquid seeped out of the samples. Some remnants of the lignin-rich second phase can be seen by examining the inside of the pores of the cross-sectional samples.

Fracture was not conducted on the MH and MRH samples, because these samples bowed significantly in the middle of the plaque, their thickness varied throughout the cross-section and their surface finish was distinctly different than the other samples. Excess water evaporated during the postcuring step and was trapped between the silicone mold and the gelled epoxy, causing a bubble, which then set into a bowed shape having

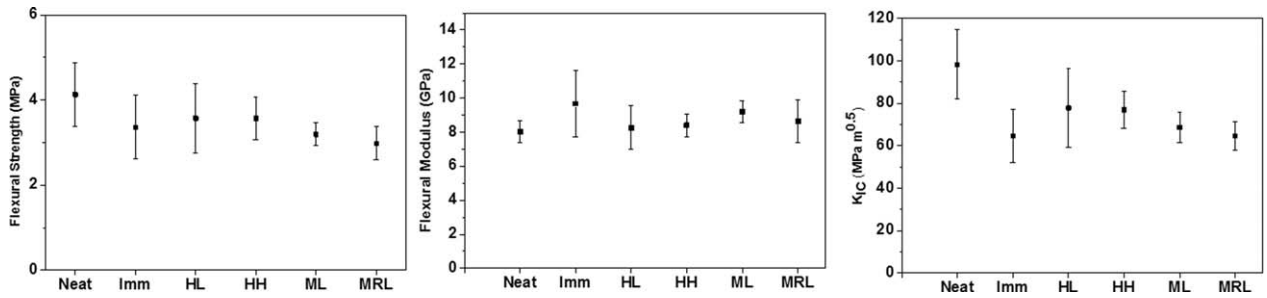

Figure 4. Flexural strength, flexural modulus, and K_{IC} of epoxy–lignin composites. The error bars represent 95% confidence intervals.

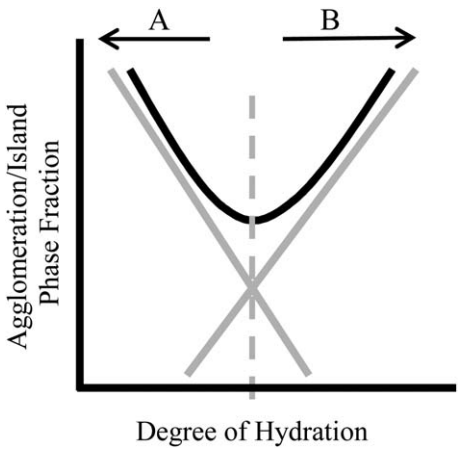

Figure 5. Schematic of the second phase volume fraction as a function of degree of hydration. Region A is dominated by lignin agglomerations, and region B is dominated by pores.

different cross-sectional areas. The water evaporation on the top surface caused a local rippling effect which decreased transparency of the sample and increased surface roughness, which may have created defects large enough to be crack nucleation sites.

The mechanical properties of the epoxy–lignin composites are shown in Figure 4. The samples show no statistically significant difference in flexural modulus and show a significant decrease in K_{IC} for all samples except HL. The flexural stress changes in the ML and MRL are significant decreases. The error bars in the neat epoxy sample can be taken as a metric for variability in sample preparation and testing.

Fracture in all samples nucleated from the notch of the sample and not from an internal flaw, indicating that the incorporation of the second phase did not strongly affect crack nucleation. Decreases in the fracture toughness were largely due to a decrease in ductility of the specimen. This decrease in ductility is also likely responsible for the increase in modulus seen in the samples.

On the basis of observation, it is likely that there is an optimal degree of hydration which will minimize both agglomeration and second phase particle size (Figure 5). Reduced agglomeration due to water addition (region A) will increase homogeneity until pores form due to excess water (region B). It is expected that the minimum is located near 0.5 wt % water.

The FTIR spectra of the various lignin samples show broad similarities with the Neat samples, with some notable chemical differences. The spectra are normalized to the 1, 4-aromatic disubstitution of the DGEBA molecule at 829 cm^{-1}. The absence of an absorption band at 915 cm^{-1} in all of the samples indicates that the epoxide rings have completely opened and the sample is cured.

There are three main regions of chemical difference in the spectra, as indicated in Figure 6 and Table II. The hydroxyl and

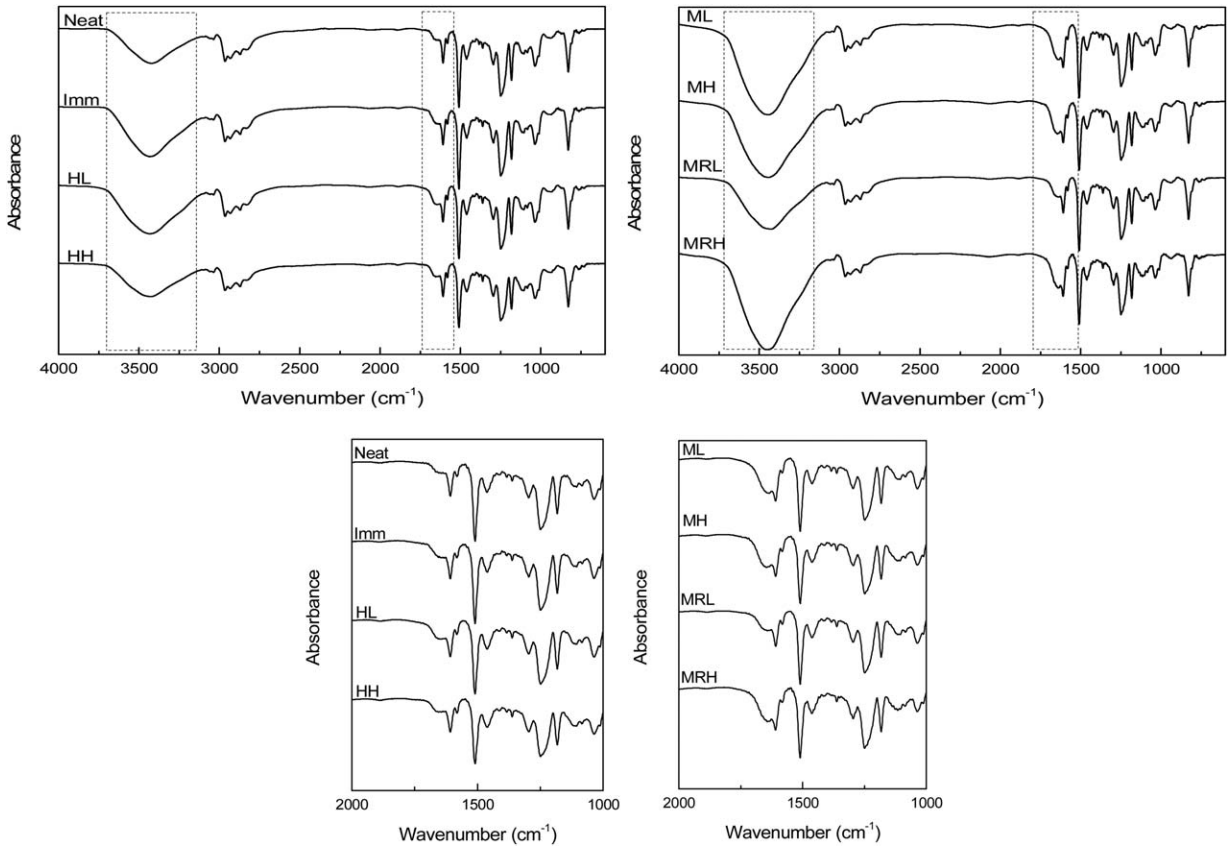

Figure 6. FTIR spectra of epoxy specimen. Regions of interest are marked by dotted boxes. The spectra are normalized to the peak at 829 cm^{-1}.

Table II. FTIR Peaks for the Lignin–Epoxy System

Wavenumber (cm^{-1})	Mode
829	Aromatic 1,4 disubstitution
1248	Aromatic ether
1610-1680	Amines and aromatic rings
2965, 2935, 2873, 2828	Methyl and methylene stretching
3300	Hydroxyl and amine

secondary and tertiary amine region (3700–3200 cm^{-1}) displays a broad peak, indicative of hydrogen bonding, which increases in intensity in the Mannich samples. The region between 1680 and 1600cm^{-1} shows the presence of secondary amine, and the peak at 1610 cm^{-1}, corresponding to the —C═C— in the aromatic ring, both exhibit a large increase in intensity for the ML, MH, and MRH samples. The regions corresponding to primary amine in the 1100–1000 cm^{-1} show a decrease in intensity corresponding to the increased reaction of primary amine in the Mannich reaction.

The DSC thermograms (Figure 7) show a significant difference between the Mannich reaction samples and other specimen. ML, MH, MRL, and MRH have a broadened, less-defined glass transition (Table III), indicative of chemical heterogeneity. The samples show a residual exotherm above 120°C, most notably in the MH and MRH samples. Upon reheating, the exotherms disappear, indicating the completion of the cure. The glass transition temperatures increase monotonically upon reheating. Water evaporation is not apparent in any of the samples, which would be indicated by an endothermic reaction above 100°C.

The Neat, IMM, HL, and HH samples undergo a glass transition with an enthalpy relaxation, upon initial heating. Although the Mannich samples do not exhibit a clear enthalpy relaxation, it is possible that it is obscured by the broadened glass transition and the onset of curing. The relaxation does not reappear during the second heating, indicating that the samples have fully relaxed.

Shifts in the glass transition temperature (Figures 7 and 8) are due to two distinct mechanisms, enthalpic relaxation[23] and plasticization.[14,24] In the NE, IMM, HL, and HH samples, an enthalpic relaxation occurs as indicated by an endotherm immediately after the glass transition. The epoxy molecules are able to move from a kinetically trapped state to a state where chain rearrangement and further bonding are promoted. In the ML and MRL, the enthalpic relaxation is largely obscured or absent.

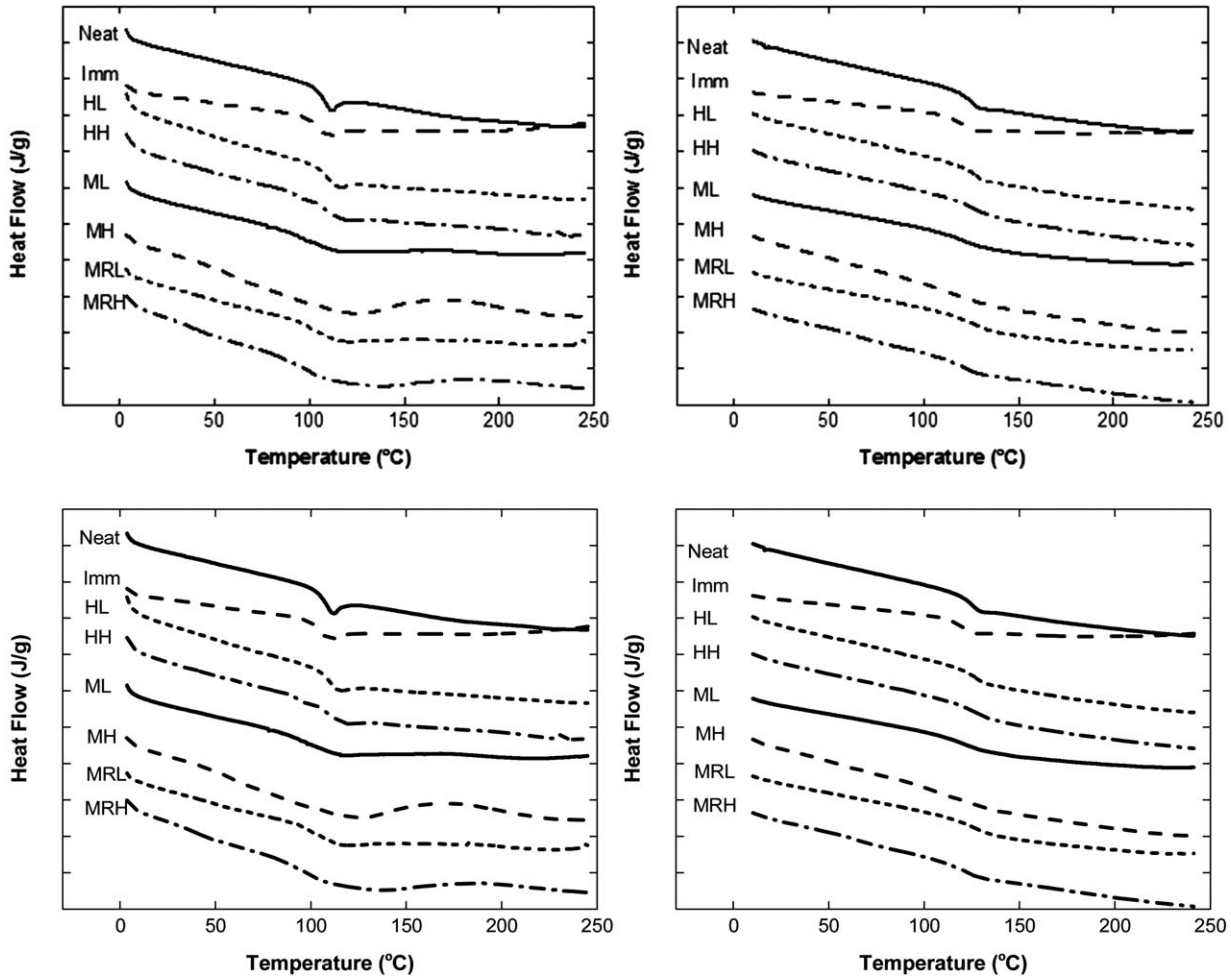

Figure 7. DSC thermograms of the first heat (left) and second heat (right) epoxy compositions.

Table III. Glass Transition of Epoxy Samples Determined Through DSC

	First heat			Second heat		
	T_g onset (°C)	T_g end (°C)	ΔT (°C)	T_g onset (°C)	T_g end (°C)	ΔT (°C)
Neat	103	109	6	121	129	8
IMM	100	107	7	115	125	10
HL	104	113	9	120	131	11
HH	98	114	16	119	132	13
ML	97	101	4	110	128	18
MH	52	86	34	97	129	32
MRL	97	106	9	117	133	16
MRH	89	108	19	116	127	11

The MH and MRH samples likewise show no enthalpic rearrangement because of sufficient plasticization, but do show evidence of postcuring, as exhibited by the peak around 160–180°C. This result is contrary to previous work[15,17,19] and shows that hydration and Mannich functionalization of lignin interferes with the curing process.

Water molecules may act as a plasticizer to increase free volume and allow the chains in the ML and MRL to reach an energy minimum. It is expected that large amounts of water reacted with the Mannich-functionalized amine groups to form hydroxyl and tertiary amine groups, as shown in the 3700–3300 cm^{-1} region of the FTIR data, and inhibited curing in the MH and MRH sample. In comparison, the cure inhibition and postcuring behavior is not seen in the HH specimen, and the intensity of the hydroxyl peak remains similar to the neat epoxy.

The large degree of postcuring suggests that the *as-tested* MH and MRH samples have a lower crosslink density than the other epoxy samples. Here, interactions between the excess water and the Mannich-reacted TETA molecules may have decreased the extent to which the epoxy could crosslink. It is believed that preferential formation of bonds between the water molecules and the Mannich-functionalized amines preclude the bonding of the Mannich sites to the available epoxy sites. Evolution of water (indicated by an endothermic reaction) is not seen upon heating or reheating, which indicates that the water is unable to escape the crosslinked structure because of either bonding of the water molecules or decreased diffusion of the water through the polymer. Furthermore, preferential segregation of the TETA molecules in or near lignin microspheres may deprive the epoxy matrix of crosslinking agents and decrease the degree of cure in the material.

The DMA data, shown in Figure 8, indicates that the Neat, IMM, HL, HH, ML, and MRL samples had similar storage moduli and a similar glass transition, as shown in Table IV. These values are also similar to those reported in literature.[25] In the ML, MH, and MRL, the glass transition region broadened appreciably compared with the Neat, as shown in Table IV. The MH and MRH samples showed an 800–1000 MPa decrease in storage modulus and a 20°C decrease in glass transition. The MH and MRH values deviated significantly from previously reported values and indicate that chemical modifications strongly change the properties of the epoxy.

The chemical homogeneity of a sample can be determined by the sharpness of the glass transitions in DSC and DMA. As the degree of modification increases, in terms of water content and Mannich reaction, the width of the glass transition correspondingly increases. The addition of the lignin, water, and Mannich-functionalized lignin decreases the density of stiff aromatic rings in the DGEBA molecules and creates locally mobile segments at lower temperatures. The Mannich samples exhibit a broader glass transition because of the inherent lack

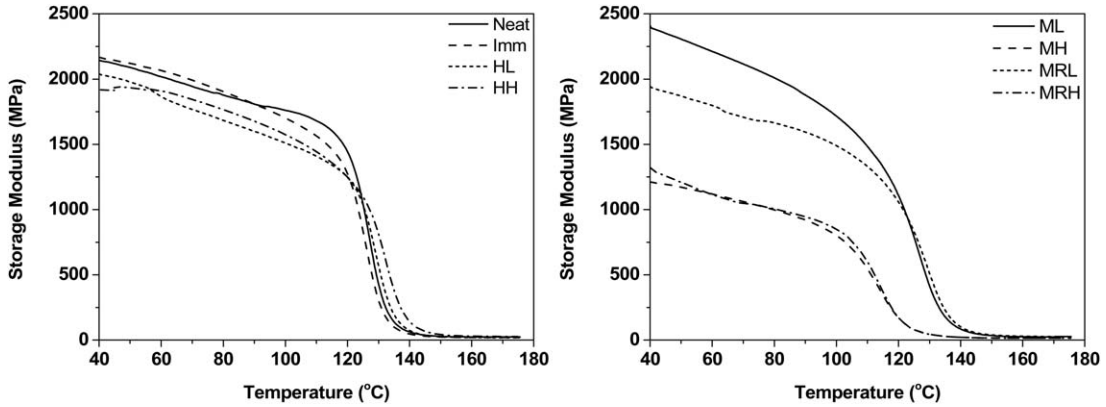

Figure 8. Dynamic mechanical properties of lignin–epoxy composites at 1 Hz.

Table IV. Storage Modulus and Glass Transition Temperature of Epoxy–Lignin Composites Determined by DMA

	Storage modulus (MPa) at 60°C	T_g onset (°C)	T_g end (°C)	ΔT (°C)
Neat	2020	121	133	12
IMM	2070	119	134	15
HL	1870	122	136	14
HH	1910	125	139	14
ML	2210	115	137	22
MH	1120	103	132	29
MRL	1800	117	139	22
MRH	1120	105	122	17

of selectivity of the Mannich reaction.[22] The Mannich reaction creates an additional methylene group between the primary or secondary amine and an available acidic proton in the lignin structure. This creates longer chains of methylene and ether bonds with lower glass transitions than the epoxy, lowering the onset temperature of the glass transition. It is notable that generally, the end temperature of the glass transition is similar in the majority of the samples, suggesting that the stiffest unit, likely the bisphenol A segment, becomes more mobile at that point.

CONCLUSIONS

Lignin was functionalized using hydration and the Mannich reaction to increase dispersion in epoxy. The morphology of the lignin-containing specimen showed the development of a lignin-rich second phase, which is formed by the phase separation of lignin and water at high temperatures. Mechanisms for phase separation were proposed. Thermomechanical properties were characterized though DMA, DSC, and fracture testing. Results of these tests showed that the glass transition temperature, storage modulus, yield stress, and elastic modulus remained similar for the HL, HH, ML, and MRL samples. The MH and MRH exhibited lower thermomechanical properties because of a strong plasticization effect which arose from a synergistic interaction between the hydration and the Mannich chemistry. Chemical analysis using FTIR showed that the Mannich-functionalized lignin specimen had increased interaction with water, as shown by the increase in the hydroxyl and tertiary amine regions at 3300–3700 cm^{-1}. Facile modification of lignin using the Mannich reaction and hydration can increase the dispersion of lignin in an epoxy matrix and provide comparable thermomechanical properties to neat epoxy. As such, lignin can be potentially be used as a sustainable fill material in epoxies.

ACKNOWLEDGMENTS

The authors gratefully acknowledge the NSF IGERT on Sustainable Electronics (DGE 1144843) for support of this research.

REFERENCES

1. Gosselink, R. J. A.; de Jong, E.; Guran, B.; Abächerli, A. *Ind. Crops Prod.* **2004**, *20*, 121.
2. Holladay, J. E.; White, J. F.; Bozell, J. J.; Johnson, D. Top Value-Added Chemicals from Biomass Volume II—Results of Screening for Potential Candidates from Biorefinery Lignin; Pacific Northwest National Laboratory, Richland, Washington, **2007**; Vol. 2.
3. Brebu, M.; Vasile, C. *Cellul. Chem. Technol.* **2010**, *44*, 353.
4. Lora, J. H.; Glasser, W. G. *J. Polym. Environ.* **2002**, *10*, 39.
5. Gellerstedt, G.; Henriksson, G. In Monomers, Polymers and Composites from Renewable Resources; Elsevier, **2008**, pp 201–224.
6. Ouyang, W.; Huang, Y.; Luo, H.; Wang, D. *J. Polym. Environ.* **2011**, *20*, 1.
7. Zhang, R.; Xiao, X.; Tai, Q.; Huang, H.; Hu, Y. *Polym. Eng. Sci.* **2012**, *52*, 2620.
8. Rahman, M. A.; De Santis, D.; Spagnoli, G.; Ramorino, G.; Penco, M.; Phuong, V. T.; Lazzeri, A. *J. Appl. Polym. Sci.* **2013**, *129*, 202.
9. Li, Y.; Mlynar, J.; Sarkanen, S. *J. Polym. Sci. B Polym. Phys.* **1997**, *35*, 1899.
10. Wang, Z.; Xue, J. W.; Qu, J. B.; Liu, W. X. *Adv. Mater. Res.* **2012**, *560–561*, 242.
11. Pouteau, C.; Baumberger, S.; Cathala, B.; Dole, P. C. R. *Biol.* **2004**, *327*, 935.
12. Pouteau, C.; Cathala, B.; Dole, P.; Kurek, B.; Monties, B. *Ind. Crops Prod.* **2005**, *21*, 101.
13. Hilburg, S. L.; Elder, A. N.; Chung, H.; Ferebee, R. L.; Bockstaller, M. R.; Washburn, N. R. *Polymer (Guildf).* **2014**, *55*, 995.
14. Hofmann, K.; Glasser, W. *Macromol. Chem. Phys.* **1994**, *80*, 65.
15. Hofmann, K.; Glasser, W. G. *J. Adhes.* **1993**, *40*, 229.
16. Hofmann, K.; Glasser, W. G. *J. Wood Chem. Technol.* **1993**, *13*, 73.
17. Feldman, D.; Banu, D.; Natansohn, A.; Wang, J. *J. Appl. Polym. Sci.* **1991**, *42*, 1537.
18. Feldman, D.; Banu, D.; Khoury, M. *J. Appl. Polym. Sci.* **1989**, *37*, 877.
19. Feldman, D.; Banu, D.; Studies, B. *J. Polym. Sci. A Polym. Chem.* **1988**, *26*, 973.
20. Liu, J.; Liu, H.-F.; Deng, L.; Liao, B.; Guo, Q.-X. *J. Appl. Polym. Sci.* **2013**, *130*, 1736.
21. Yue, X.; Chen, F.; Zhou, X. *BioResources.* **2011**, *6*, 2022.
22. Pan, H.; Sun, G.; Zhao, T. *Int. J. Biol. Macromol.* **2013**, *59*, 221.
23. Montserrat, S. *J. Polym. Sci. B Polym. Phys.* **1994**, *32*, 509.
24. Ciemniecki, S.; Glasser, W. In Lignin Properties and Materials; American Chemical Society, **1989**, pp 452–463.
25. Dang, D. N.; Cohendoz, S.; Mallarino, S.; Feaugas, X.; Touzain, S. J. *Appl. Polym. Sci.* **2013**, *129*, 2451.